Materials Today Bio 29 (2024) 101368

Contents lists available at ScienceDirect

Materials Today Bio

journal homepage: www.journals.elsevier.com/materials-today-bio

Injectable hyaluronate-L- cysteine gel potentiates photothermal therapy in osteosarcoma via vorinostat-copper cell death

Sizhen Wang [a,1], Hanzhe Zhang [b,1], Tianheng Chen [a,1], Weiwei Jiang [a], Feng Wang [b], Yuhao Yu [b], Beibei Guo [a], Jia Xu [b,**], Feng Yang [a,c,***], Qinglin Kang [b,****], Zhiqiang Ma [a,*]

[a] Department of Inorganic Chemistry, Pharmacy School, Naval Medical University, 325 Guohe Road, Shanghai, 200433, People's Republic of China
[b] Department of Orthopaedic Surgery, Shanghai Sixth People's Hospital Affiliated to Shanghai Jiao Tong University School of Medicine, Shanghai, 200233, People's Republic of China
[c] Department of Nuclear Medicine, Shanghai Fourth People's Hospital, School of Medicine, Tongji University, Shanghai, 200434, People's Republic of China

ARTICLE INFO

Keywords:
Cuproptosis
Osteosarcoma
Injectable hydrogel
Phototherapy
Vorinostat

ABSTRACT

The prognosis for osteosarcoma patients, a devastating malignancy affecting young individuals, remains grim despite multimodal therapeutic advances. Recently, the advent of cuproptosis, a novel programmed cell death, offers hope in fighting osteosarcoma. In this study, we introduce $SAHA_m$@$\{[Cu(HA\text{-}Cys)_2]Cl_2\}_n$, an injectable hyaluronate-L-cysteine hydrogel that integrates both copper ions (Cu^{2+}) and vorinostat (SAHA) for the possible therapeutic effect. The Cu^{2+} targets the TCA cycle, inducing cuproptosis in osteosarcoma cells. While SAHA acts as both a histone deacetylase inhibitor and an ROS generator for eliminating tumor cells. The mechanism involves amplifying FDX-1 expression via SAHA modulation of the TCA cycle, which was an original discovery. Critically, the combined mechanisms and localized injection enables the hydrogel partially eradicating osteosarcoma without metastasis in rats. Therefore, this study advances cuproptosis induced photothermal therapy for promising clinical translations, shedding light on favorable prognosis for osteosarcoma.

1. Introduction

Osteosarcoma, a rare cancer in 0-19-year-olds, has an annual incidence of 4.6–5.0/million [1], increasing notably from 1975 to 2017, peaking recently [2]. Despite chemotherapy advancements raising 5-year survival from 20 % to 70 %, relapse and metastasis remain obstacles [3–6]. A quarter of patients develop lung metastasis at diagnosis, emphasizing the need for better treatments. Combination therapies like chemo, immuno [7], photothermal [8] and ablation show promise but tumor-free outcomes are elusive. Neoadjuvant chemo improves relapse-free survival (RFS)but is limited by resistance, toxicity, and rapid clearance. Therefore, Drug-delivering platforms to minimize side effects and improve prognosis are lacking in practice. Studies implicate PI3K/mTOR [9,10], WNT/β-catenin [11,12], and RANKL/NF-κB [13] in driving tumor cell proliferation, chemoresistance, and early metastasis [14]. Genomic loss of TP53 and RB inactivation are common in osteosarcoma cells [15]. Unfortunately, targeted therapies within drug-delivering platforms for these pathways have limited success at present [14].

Cuproptosis, a new cell death pathway, offers hope for osteosarcoma patients by extending RFS. This pathway targets lipoylated TCA cycle [16–18] and Fe-S cluster proteins [19], disrupting mitochondrial respiration and causing proteotoxic stress. Studies have shown conserved lysine modification regulates carbon entry in the TCA cycle, occurring on Dihydrolipoamide Branched Chain Transacylase E2 (DBT), Glycine Cleavage System Protein H (GCSH), Dihydrolipoamide S-Succinyltransferase (DLST), and Dihydrolipoamide S-Acetyltransferase (DLAT) [20,21]. Among them, Ferredoxin (FDX-1) is a key upstream regulator of cuproptosis-induced cell death, emphasizing its potential in cancer therapy.

* Corresponding authors.
** Corresponding author.
*** Corresponding author. Department of Inorganic Chemistry, Pharmacy School, Naval Medical University School, 325 Guohe Road, Shanghai, 200433, People's Republic of China.
**** Corresponding author.
E-mail addresses: xujia0117@sjtu.edu.cn (J. Xu), yangfeng1008@126.com (F. Yang), orthokang@163.com (Q. Kang), briskbreeze@126.com (Z. Ma).
[1] These authors contributed equally to this work.

https://doi.org/10.1016/j.mtbio.2024.101368
Received 9 September 2024; Received in revised form 1 November 2024; Accepted 23 November 2024
Available online 23 November 2024

Cuproptosis shows promise in cancer therapy, yet challenges limit its clinical potential. Cuproptosis as a standalone treatment may not fully eradicate tumor cells [16], requiring exploration of combinatorial strategies with other therapies like radiation, chemotherapy, phototherapy, and immunotherapy. Additionally, copper overload risk necessitates careful consideration in utilizing cuproptosis benefits. Addressing challenges is key to advancing cuproptosis in cancer management. Based on our current understanding, incorporating additional therapies with reduced copper may enhance cuproptosis effectiveness. Considering the favorable photothermal conversion efficacy of copper hydrogel, photothermal therapy is a highly suitable approach.

Intracellular copper levels are maintained low by conserved homeostatic mechanisms mediated by copper-binding ionophores (SLC31A1, ATP7A, ATP7B) [22–24]. Ionophores regulate copper influx and efflux, ensuring tight control over cellular copper levels. However, this precise copper regulation poses a challenge: extracellular copper can become toxic before reaching therapeutic intracellular levels. Fortunately, CD44, a hyaluronate receptor, enhances copper uptake, implicating hyaluronate acid as a potential platform for targeted tumor delivery [25,26].

Chemotherapy, as adjuvant/neoadjuvant, improves survival when combined with surgical resection of tumor/limbs [27–29]. Osteosarcoma treatment commonly includes drugs like doxorubicin, cisplatin, cyclophosphamide, etc. [30,31] Recent studies show SAHA enhances doxorubicin and cisplatin cytotoxicity in osteosarcoma cell lines [32]. SAHA's immunological mechanisms are unclear, but its ROS generation positions it as a potential novel osteosarcoma chemotherapy option [33]. SAHA augments radiation response in osteosarcoma and rhabdomyosarcoma cell lines, highlighting its versatility [34,35]. However, further research is needed to unravel SAHA's immunological therapeutic pathways.

Herein, we propose integrating SAHA into a hyaluronic acid hydrogel for cuproptosis-based osteosarcoma therapy (Scheme 1) [32,36,37]. SAHA is not only a histone deacetylase inhibitor (HDAC inhibitor), but also an ROS generator for tumor cell elimination. In our study, SAHA and Cu^{2+} both are therapeutic molecular loaded in a hyaluronate-L-cysteine hydrogel. Remarkably, our study uncovers SAHA's mechanism, stimulating FDX-1 and lipoylated TCA cycle proteins. This finding advances therapeutic potential of cuproptosis in osteosarcoma regression and metastasis prevention, deepening understanding of copper-induced cell death via lipoylated TCA proteins [16].

2. Materials and methods

2.1. Materials

Sodium hyaluronate (HA, 200 kDa) was purchased from Yunmo Biotechnology (Shanghai) Co. Ltd, t-butyloxy carbonyl-L-cysteine (BOC-L-Cys), 1-(3-Dimethylaminopropyl)-3-ethylcarbodiimide (hydrochloride) (EDC·HCl), 1-Hydroxybenzotriazole (HOBT), Trifluoroacetic acid (TFA) were obtained from Adamas Co. Ltd (Shanghai). Vorinostat (SAHA, Cat no.8638-EG-050) was purchased from R&D Systems Inc., Minneapolis, MN, USA.

2.2. Fabrication and characterization of CHASA hydrogel

The injectable hyaluronate-L-cysteine hydrogel was fabricated and characterized as described in supplementary materials.

2.3. Anti-tumor effect of CHASA hydrogel in vitro

2.3.1. Experimental investigation of cellular effects

Cell culture, *in vitro* cytotoxicity assay, cell apoptosis and intracellular ROS level were conducted as ordinary protocols as described in supplementary materials.

2.3.2. Quantitative real-time PCR analysis

Total RNA was extracted using the EZ-press RNA Purification Kit (B0004D-100; EZBioscience, USA), following which reverse transcription was carried out employing a cDNA Reverse Transcription Kit (EZBioscience, USA) in a strict adherence to the manufacturer's protocol. Quantitative analysis was then performed, employing SYBR Green I Master Mix (EZBioscience, USA) along with a LightCycler® 480 Real-

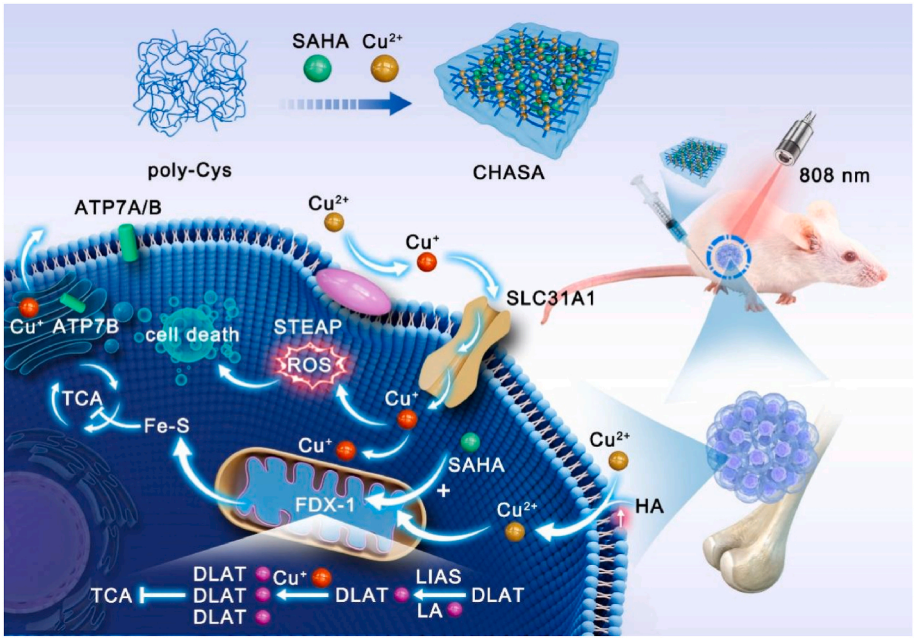

Scheme 1. An Illustrative Depiction of the Fabrication of CHASA and Its Promising Anti-Tumor Mechanism, Featuring Cuproptosis Potentiated by Copper-Death Enhancer SAHA and Photothermal Effect Triggered by 808 nm near-infrared laser. Abbreviations: poly-Cys (hyaluronate-L-cysteine hydrogel precursors, poly-HA-Cys), SAHA (Vorinostat), CHASA (SAHAm@{[Cu(HA-Cys)$_2$]Cl$_2$}n hydrogel), SLC31A1(Solute Carrier Family 31 Member 1), ATP7A/B(Copper-transporting P-type ATPase) , TCA cycle (Tricarboxylic Acid Cycle), DLAT (Dihydrolipoamide S-Acetyltransferase) , LIAS(Lipoic Acid Synthase) , LA (Lipoic Acid).

time PCR system (Roche, Basel, Switzerland). The qPCR primers were obtained from Beyotime (Shanghai, China).

2.3.3. Western blot analysis

Cells diluted 1:4 with 5 × loading buffer, heated at 95 °C for 5 min. Protein extracts separated by 7.5 %, 10 %, or 15 % SDS-PAGE and transferred to PVDF membranes. Membranes blocked with 5 % non-fat milk for 2 h. Subsequently, PVDF membranes incubated overnight with primary antibodies against FDX-1 (1:1000, Abcam) and DLAT (1:1000, CST). Membranes washed 3times in TBST buffer and incubated with HRP-conjugated secondary antibodies for 1 h at RT. Immunoreactive bands visualized using ECL kit (SQ201) and detected with ChemiDoc Imaging System. GAPDH used as protein loading control.

2.3.4. Transwell assay of UMR106 and U2OS

Approximately 5 × 10^4 UMR106/U2OS cells seeded into wetted Transwell insert (Corning, 8.0 μm). Added 500 μl complete medium (10 % FBS) to lower chamber. After 24 h incubation, aspirated medium and fixed cells with 4 % PFA for 15 min, rinsed with ddH_2O twice. Removed residual cells from upper chamber with sterile swab. Stained remaining cells with 0.5 % crystal violet for 10 min, washed with ddH_2O twice.

2.3.5. The polarization of RAW264.7 cells assessment

RAW264.7 cells were seeded at 1.0 × 10^6/well in 6-well plates. After overnight incubation at 37 °C, cells were grouped into control, HA, CHA, and CHASA (with/without radiation). Each group was stained with PE anti-mouse CD86 (Biolegend, 105105) and APC anti-mouse CD206 (Biolegend, 141707). Flow cytometry was performed to assess RAW264.7 polarization post-staining.

2.4. Regression and anti-metastasis of osteosarcoma in vivo

2.4.1. Rat osteosarcoma model and animal experiments

The rat osteosarcoma model was approved by the Animal Care Committee of Naval Medical University. The male SD rats were anesthetized with 0.3 % barbiturate (1 ml/100 g BW). The surgical site was then prepared by shaving the fur and sterilizing the area with 75 % alcohol. Initially, a suspension containing 4 × 10^6 UMR106 cells in 200 μL of PBS was injected subcutaneously into the tibia region of each SD rat. 8 days later, rats were randomly assigned to saline, CHA, CHASA, or CHASA + NIR groups (n = 5). Tumor growth was closely monitored and documented without further surgical interventions. On day 0, hydrogel was injected concurrently with grouping. Tumor volume and rat body weight were consistently measured and recorded every 3 days for each group. In addition, another 6 rats were used to study the survival curve. Tumor volume was calculated using a standard formula:

$$\text{Tumor volume (V)} = (\text{Tumor length}) \times (\text{Tumor width})^2/2$$

On day 15, all the rats were euthanized, tumor tissues and the lungs were harvested for further evaluation.

2.4.2. Immunohistochemistry

Tumor samples were fixed with 4 % PFA to preserve structural integrity. H&E staining visualized tissue architecture and cellular morphology. In parallel, frozen tumor tissues were sectioned into thin slices from each group. TUNEL staining (30 μM) quantified apoptosis levels under a fluorescence microscope. IHC sections were pretreated with 0.3 % H_2O_2 for 20 min to eliminate peroxidase. Antigen retrieval in citrate buffer (pH 6.0) at 65 °C for 20 min enhanced accessibility. Blocking with 5 % goat serum for 1 h minimized nonspecific binding. Subsequently, sections were incubated with primary antibodies overnight at 4 °C. Following this, sections were exposed to HRP-conjugated secondary antibodies for 1 h at 25 °C.

2.4.3. Histology for immunofluorescence staining

Tissue sections underwent dewaxing, antigen retrieval for IF staining, similar to IHC. Permeabilized with 0.1 % Triton X-100 for 20 min to allow antibody access. Blocked with 5 % BSA for 1 h at RT. Incubated with primary antibodies overnight at 4 °C for antigen recognition. After PBS wash, treated with secondary antibodies and DAPI for nuclear staining. NIKON ECLIPSE C1 system quantified positive staining, revealing tumor tissue characteristics.

2.5. Statistical analyses

The data were shown as mean ± standard deviation. For multiple-group analyses, a one-way analysis of variance (ANOVA) was conducted, followed by Tukey's post hoc test.

3. Results and discussion

3.1. Characterization of CHASA hydrogels

By dropwise adding Cu^{2+} to HA-Cys polymers (HA) at pH 7.4, the hydrogel cross-links via Cu^{2+} ions and amido/carboxyl groups into pentacyclic chelates (Fig. S1), and formed a porous hydrogel (CHA) as Fig. 1A and 1C showed. Notably, SAHA is incorporated into Cu^{2+} crosslinking in CHASA hydrogel, yielding a hydrogel of SAHA and sodium hyaluronate-L-cysteine.

SEM and EDS assessed crosslinking density and hydrogel network disparities between HA and Cu^{2+}. 10%-CHA hydrogel had the most compact structure due to higher crosslinking density with Cu^{2+}. EDS elemental mapping showed distributions in 3 %, 5 %, and 10%-CHA hydrogels (Fig. 1B). Accordingly, viscosity rise could be well observed during Cu^{2+} addition (Fig. 1C). In order to study the rheological properties of CHA hydrogels, we selected 10%-CHA hydrogels for verification. Frequency sweep confirmed hydrogel formation with much higher G' than G'', reflecting its elasticity and stability, and indicating the successful preparation of the injectable CHA hydrogel (Fig. 1D). Additionally, step strain sweep showed CHA hydrogel's self-healing after 4 cycles (Fig. 1E). ^1H NMR examined CHA structural characteristics (Fig. S2A). FT-IR spectrum showed the peak at around 3000 cm^{-1} belonged to -NH_2 stretching from L-cysteine, while the peak at about 3600 cm^{-1} attached to N-H stretching [38], both verifying the synthesis of CHA (Fig. S2B).

The injectability of hydrogel was depicted in Fig. 1F, demonstrating the viscosities of CHA hydrogel underwent a notable reduction with escalating shear rate. Swelling test revealed that 10%-CHA hydrogel displayed the lowest swelling rate, consistent with observations made in neutral and weak acidic environments (pH 7.4 and 6.5), which was suitable for intratumoral or intratissue injection because it did not impose additional negative pressure on the tissue (Fig. 2A). Because of this, we chose 10%-CHA for the following degradation research. The stability of the 10%-CHA hydrogel was assessed following immersion in PBS at pH 6.5 and 7.4. As illustrated in Fig. 2B, a notable weight loss was observed within 24 h, with degradation rate reaching 82.8 % and 77.1 % in PBS at pH7.4 and 6.5 respectively, indicating the acceptable biodegradation profile of CHA *in vivo* for tumor therapy.

3.2. Photothermal effect of CHA and CHASA hydrogels in vitro

As illustrated in Fig. 2C, the temperature of 10%-CHA hydrogel increased from 17.65 °C to 43.92 °C under NIR laser irradiation within just 4 min. In comparison, water experienced a much smaller temperature increase (from 18.68 to 28.02 °C). However, the 3%- and 5%-CHA hydrogels didn't reach temperature above 40 °C after 4 min of radiation (3%-CHA was from 16.22 °C to 35.98 °C, 5%-CHA was from 17.74 °C to 38.38 °C), their relatively poor photothermal performance rendered them unsuitable for tumor photothermal therapy. Therefore, we chose 10%-CHA hydrogel for the subsequent experiments.

The photothermal effect of 10%-CHASA hydrogel loaded with SAHA

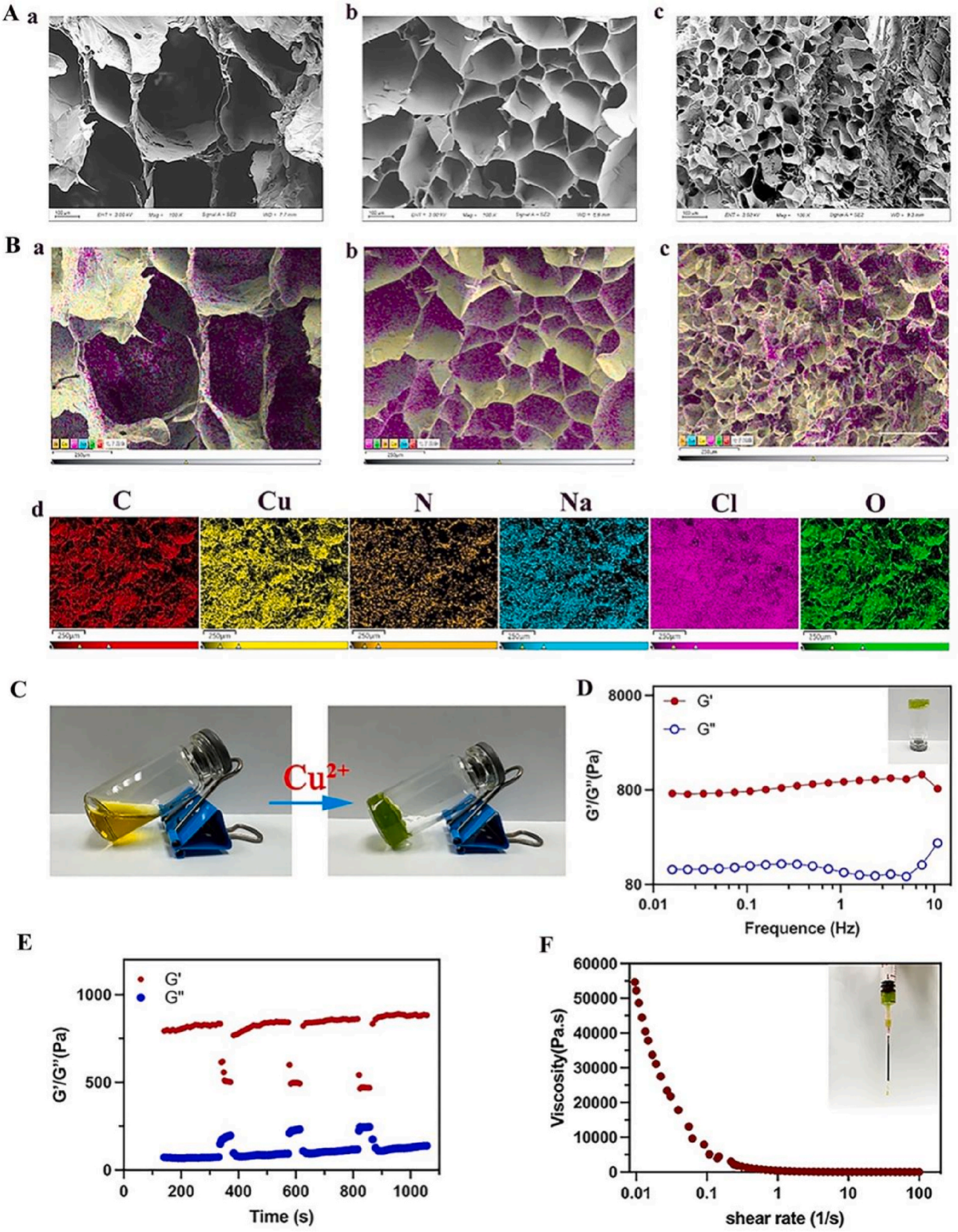

Fig. 1. (A) The scanning electron microscope (SEM) images of a) 3%-CHA, b) 5%-CHA and c) 10%-CHA hydrogels. Scale bar: 100 μm. (B) Element mapping analysis of a) 3%-CHA, b) 5%-CHA and c) 10%-CHA hydrogels; d) distribution of each element of 10%-CHA hydrogel. Scale bar: 250 μm. (C) Photographs of CHA hydrogel preparation in the presence of Cu^{2+}. The storage modulus (G′) and loss modulus (G″) of frequency sweep test (D), step strain sweep test (E) and static shear rate sweep test (F) of 10%-CHA hydrogel.

showed that the drug loading had negligible effect on photothermal performance (17.80–43.60 °C, Fig. 2C). Meanwhile, 10%-CHASA hydrogel showed outstanding photothermal stability over five cycles (Fig. 2D), with temperature maintained at the same level after intermittent laser irradiation. Hence, such characteristic made 10%-CHASA hydrogel promising for photothermal therapy.

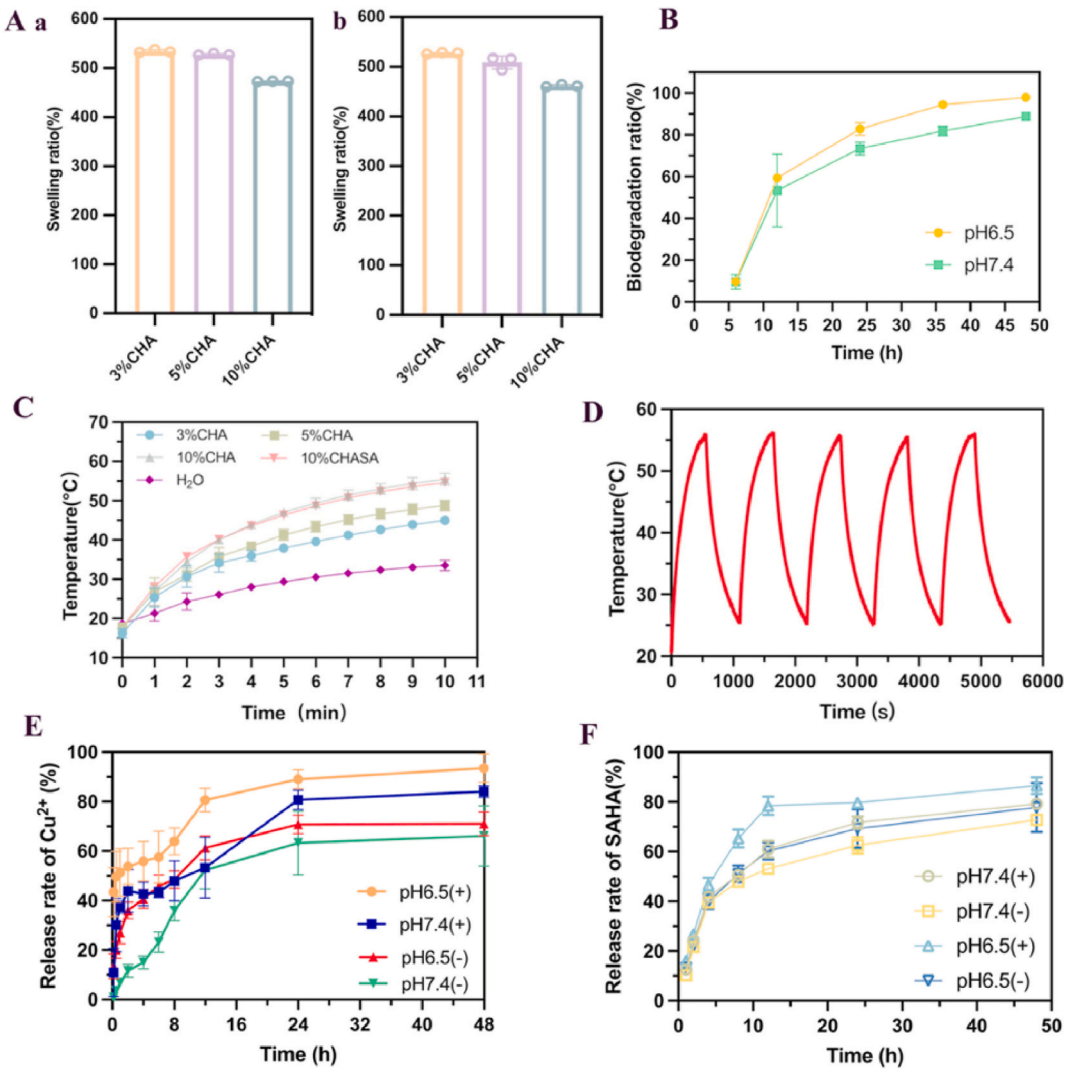

Fig. 2. (A) Swelling test of CHA hydrogels. (B) Degradation test of 10%-CHA hydrogels under different environments at room temperature (a: pH6.5, b: pH7.4). (C) The photothermal effect profile and infrared thermal of hydrogels after laser radiation for 10 min. (D) The photothermal cycling test of 10%-CHASA under the NIR light irradiation (808 nm, 1 W cm^{-2}). (E) Cu^{2+} and (F) SAHA release from 10%-CHASA hydrogel with or without NIR irradiation at pH 7.4 and 6.5 *in Vitro*. The data shown as means ± SD (n = 3).

3.3. Drug release from CHASA hydrogel in vitro

The releases of Cu^{2+} and SAHA from CHASA were examined under varying pH conditions (pH 7.4 and 6.5) both with NIR irradiation for 4 min or without that (Fig. 2E and F). The findings revealed that, after 48 h, the accumulative release of SAHA at pH 7.4 was 71.80 ± 3.47 % without NIR irradiation, while it was 72.78 ± 1.82 % at pH 6.5. Similarly, the release of Cu^{2+} was 66.16 ± 12.17 % at pH7.4 and 71.05 ± 4.78 % at pH 6.5 without NIR irradiation. This suggests that both SAHA and Cu^{2+} could be effectively released from hydrogel in both neutral (pH 7.4) and acidic (pH 6.5) environments.

It was worthing that NIR laser irradiation significantly enhanced the release of SAHA and Cu^{2+} in both neutral and acidic environments. Specifically, under NIR irradiation, the accumulative release of SAHA at pH 6.5 was 86.58 ± 3.71 % within 48 h, compared to 71.80 ± 6.24 % without irradiation, while the accumulative release of Cu^{2+} was 93.57 ± 5.83 % *vs.* 71.05 ± 4.78 %. These findings suggested that NIR irradiation could enhance the release of both SAHA and Cu^{2+} by inducing local hyperthermia, which destabilized the hydrogel network and coordination bonds, thereby facilitating the efficient release of payloads.

3.4. In vitro antitumor effects of CHASA hydrogel

Cell viability of different cell lines was detected to assess the antitumor effect of CHASA hydrogels (HA, HASA, CHA, CHASA, CHASA + laser). In this assay, the HA group was equal to the CHA group with a Cu^{2+} concentration of 0, the HASA group correspond to the CHASA group with a Cu^{2+} concentration of 0. As shown in Fig. 3A–C, HA-treated cells showed comparable survival to untreated controls, demonstrating the biocompatibility of hydrogel precursors, while CHA and CHASA hydrogels significantly decreased cell survival, especially when the concentration of Cu^{2+} more than 25.5 μM in U2OS and UMR106 cell lines, indicating their significant antitumor ability. Under the 808 NIR irradiation, our copper-ionized hydrogel exhibited a remarkable antitumor effect at a copper ion concentration of 12.75 μM compared to the hydrogel precursors (HA and HASA) with irradiation in various cell lines, suggesting the induction of photothermal effects and cuproptosis mediated by copper ions. Notably, the IC_{50} of CHASA + laser group (13.79 ± 0.76 μM for C_{Cu2+}) decreased by 1.10-fold in UMR106 cell line compared to that observed in the CHASA group (15.16 ± 1.02 μM for C_{Cu2+}), by 2.39-fold in U2OS (9.76 ± 0.68 *v.s* 23.32 ± 2.78 μM for C_{Cu2+}) and 1.19-fold in Saos-2 (29.92 ± 0.83 *v.s* 35.67 ± 7.65 μM for C_{Cu2+}) cell lines, demonstrating the enhanced photothermal effect of our

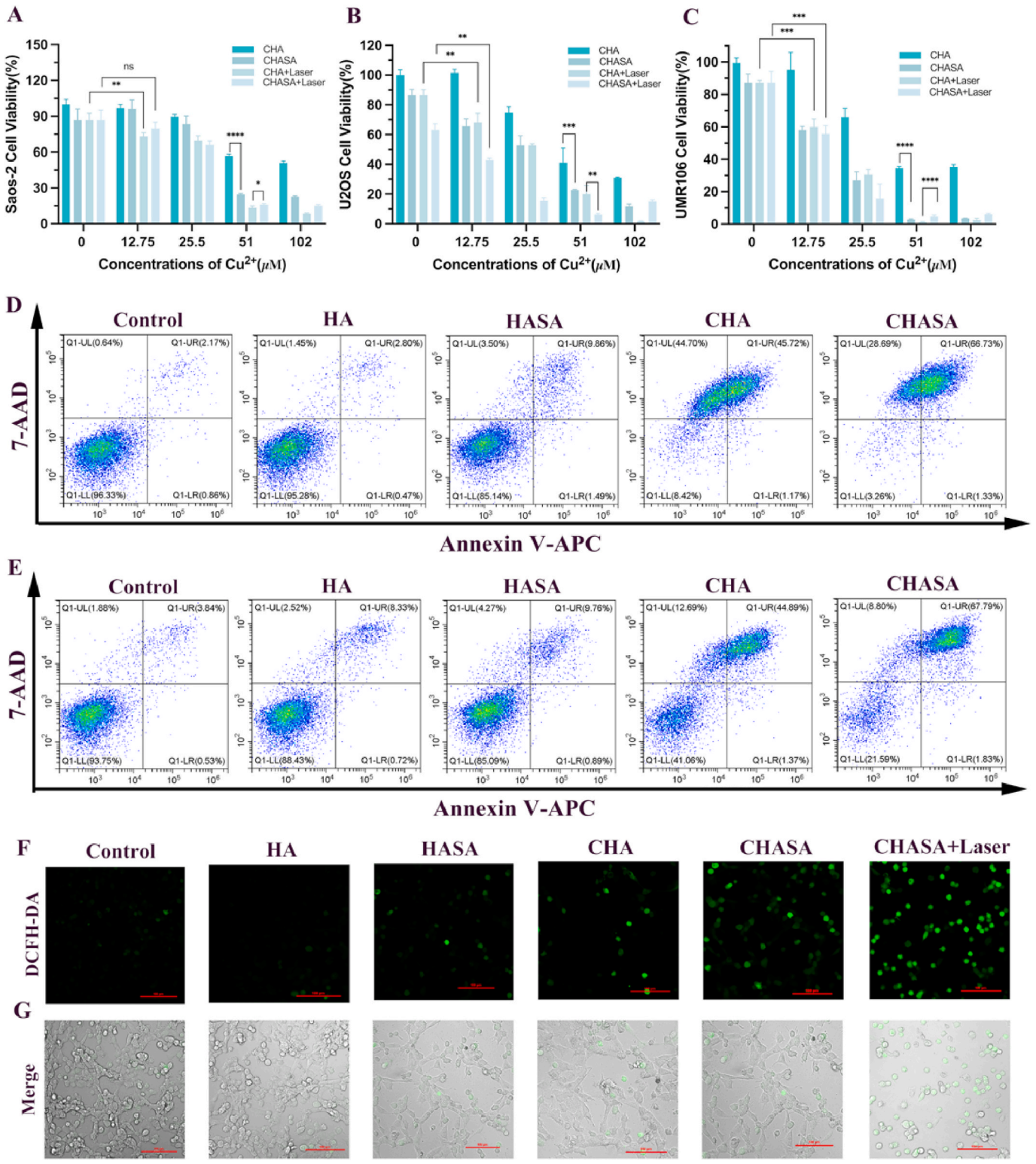

Fig. 3. MTT assessment of tumoricidal activities of hydrogels with/without radiation (NIR light irradiation, 808 nm, 1 W/cm^2). The tests were conducted with (A) Saos-2, (B)U2OS, and (C)UMR106 cell lines. Apoptosis analysis of UMR106 (D), Saos-2 (E) treated with HA, HASA, CHA, CHASA accordingly compared with the control group. (F) Fluorescent confocal images of intracellular ROS generation in Saos-2 cell lines after incubation with PBS, HA, CHA, CHASA, CHASA separately by using DCFH-DA dye. (G) Merging of fluorescent confocal images and optical images under microscope. Scale bar: 100 μm. Data in (A), (B) and (C) are shown as mean ± SD (n = 3). Significant differences among groups were determined by one-way ANOVA and post hoc Dunnett's test; *p < 0.05; **p < 0.01; and ***p < 0.001.

copper-ionized hydrogel. Additionally, regardless of laser treatment, the CHASA group was more effective than the CHA group, with a similar trend for HASA and HA, suggesting a synergistic effect between SAHA and hydrogel, enhanced by infrared light.

Cells were stained with AnnexinV-APC and 7-AAD to detect apoptotic cells in various phases by flow cytometry. As shown in Fig. 3D, both CHA and CHASA gel groups induced early (7.07 %, 6.71 % respectively) and late apoptosis (50.28 %, 59.43 % respectively).

Notably, upon treatment with CHASA gel, a remarkable 59.43 % of cells progressed into late apoptosis.

To assess ROS generation by CHA and CHASA gels, Saos-2 cells were stained with DCFH-DA and observed under a confocal microscope. Fig. 3F and **G** showed elevated ROS levels in CHA and CHASA-treated cells compared to control and HA. ROS increase attributed to Cu (II)-mediated ·OH generation via Fenton-like reactions [39,40]. Notably, the CHASA + laser group exhibited the most pronounced generation of ROS, which may be attributed to SAHA's function preset that was released completely due to hydrogel fracturing induced by photothermal effect.

3.5. Molecular mechanism of CHASA's antitumor activity in vitro

As studies suggested, cell death by copper involves Fenton's reaction, ROS, Fe-S clusters, and enzyme lipoylation. A basic framework of the key enzyme alterations in the early stages of death was established by comparing the signals and protein changes of different groups applied with comparable materials, which were opposite to the findings of several studies on terminal death changes, then we focused on antitumor mechanisms of CHA & CHASA gels.

In Fig. 4A, genes related to lipoic acid pathway (FDX-1, LIPT1, etc.) and lipoylation targets (PDHA1, PDHB) were upregulated in HASA, CHA, CHASA vs. control and HA. Additionally, Combined hydrogel treatment upregulated GCSH, LIPT1, downstream signals of lipoic acid metabolism. It is known contrasting late-phase depletion of lipoylated/Fe-S proteins, early cuproptosis upregulates lipoic acid pathway, hence, early protective mechanisms against cuproptosis in osteosarcoma cells was stressed by copper-overloaded environment. Significantly, SAHA in HASA gel upregulates FDX-1, enhancing early cell death and cuproptosis.

We analyzed protein expression levels related to cuproptosis and apoptosis (Fig. 4B and C; uncropped gels in Fig. S3). Coherently, Caspase-3 levels remained unchanged in CHASA group. However, BAX expression altered in CHASA hydrogel compared to others. This observed difference may be due to SAHA enhancing ROS generation by the copper ionized hydrogel, leading to significant apoptosis.

Numerous studies have reported that Cu-based therapy triggers cuproptosis regulated by FDX-1. In our study, we examined FDX1 and

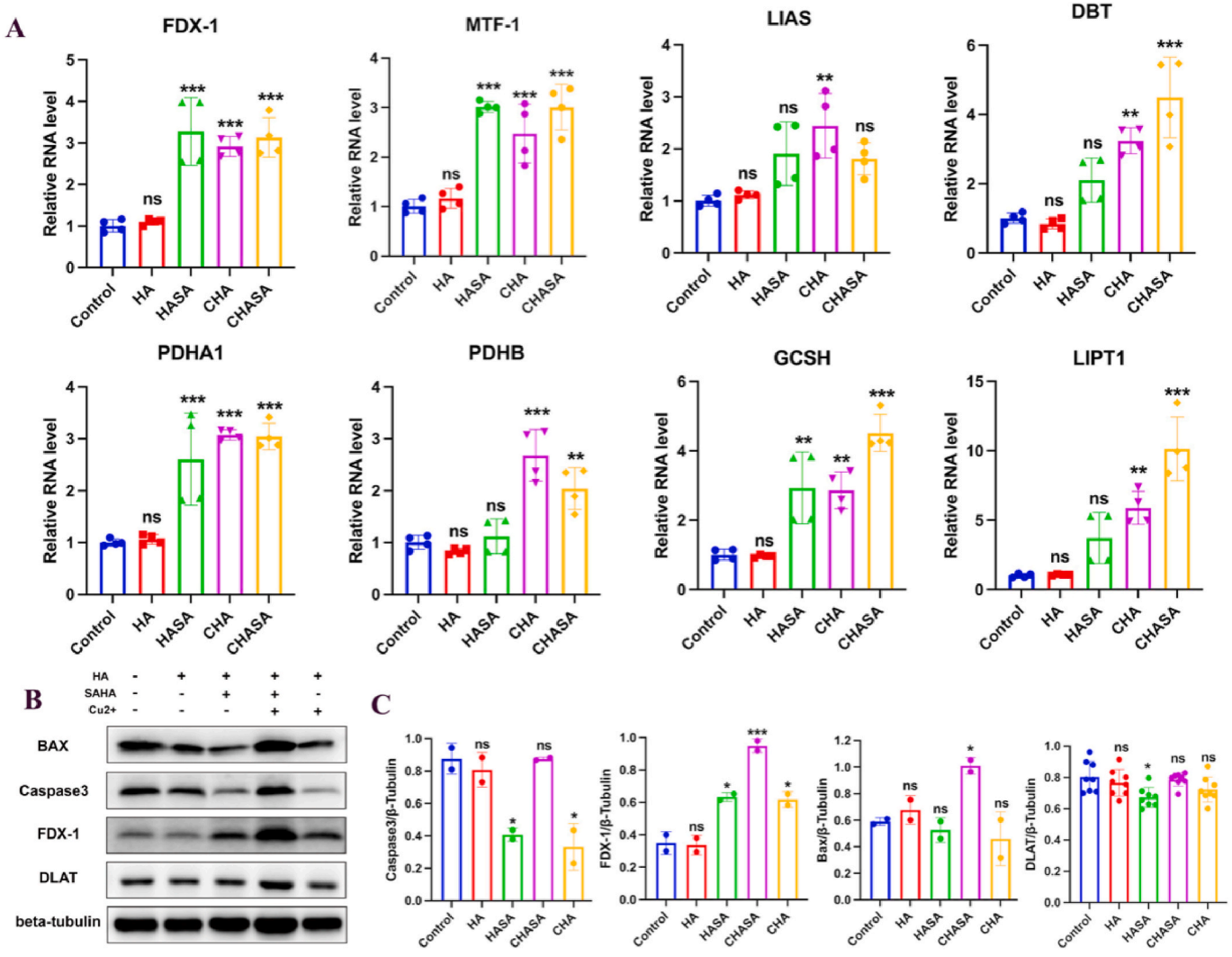

Fig. 4. (A) Expression levels of FDX-1, MTF, LIAS, DBT, PDHA1, PDHB, GCSH and LIPT1 genes in U2OS treated with control, HA, HASA, CHA, CHASA separately for 1 day, as evaluated by RT-PCR. The housekeeping gene GAPDH served as an internal control. (B) Western blots of lysates from U2OS treated with control, HA, HASA, CHA, CHASA separately. Blots were probed with antibodies against apoptosis related markers (BAX, Caspase3) and cuproptosis related markers and pathway markers (DLAT, FDX1). β-Tubulin is set as loading control. (C) Quantitation of relative protein concentration in U2OS treated with indicated hydrogels. With the data shown as means ± SD. Significant differences among groups were determined by one-way ANOVA and post hoc Dunnett's test; *$p < 0.05$; **$p < 0.01$; and ***$p < 0.001$. All immunoblots were cropped from the original here and in subsequent figures. Experimental U2OS were treated with the indicated materials. Control and experimental conditions for all functional assays were the same, except controls.

DLAT protein levels in early cuproptosis via Western blot and qPCR, and both assaies showed FDX-1 levels elevated in CHA, further in HASA. All these results suggested that SAHA-loaded hydrogel stresses osteosarcoma cells in early cuproptosis. Notably, the expression level of FDX-1 was significantly upregulated in CHASA group, suggesting its reliable activation of cuproptosis-related early signals. Studies had shown Cu^{+}-driven DLAT oligomerization was crucial for cuproptosis [41,42]. Interestingly, the total expression level of DLAT remained unchanged across all experimental groups, indicating that DLAT oligomerization may only occur in the late stage of cuproptosis.

In summary, SAHA can stimulate cuproptosis-related signals, such as FDX-1, MTF, LIAS, DBT, PDHA1, PDHB, GCSH, and LIPT1. The combined CHASA hydrogel eliminates cancer cells via cuproptosis and apoptosis. The synergy amplifies effects by activating ROS generation and stressing lipoic acid metabolism, and the later mechanism so far seems a new finding.

3.6. *In vivo* antitumor activity

The *in vivo* photothermal performance of CHASA hydrogel at the tumor site was verified using near-infrared imaging. Fig. 5A showed CHASA hydrogel's significant temperature increase under 808 nm NIR (1W/cm^2, 4 min), outperforming HASA, indicating copper's excellent photothermal conversion. CHASA hydrogels' antitumor efficacy *in vivo* was investigated through combined chemo-photothermal therapy. In this therapy, copper and SAHA were expected to be effectively released. Initially, a rat bone tumor model was established, with rats divided into control, CHA, CHASA, CHASA + laser groups. Without surgical removal of tumors, gels were administered every 3 days starting from Day 0, and tumor growth was closely monitored (Fig. 5B).

Fig. 5C and **D** shows rapid tumor growth in the control group, while it was significantly slower in the CHA, CHASA and CHASA + laser groups, indicating their substantial inhibitory effect on tumor progression. Remarkably, in the CHASA + laser group, tumor sizes peaked on day 3 and decreased, indicating effective antitumor response. On day 15, CHA and CHASA hydrogel-treated rats showed reduced tumor size or regression (Fig. 5C), and the tumor weight of the CHA, CHASA, and CHASA + groups exhibited a significant decrease compared to the Control group (Fig. 5E). Notably, no rat died in the CHASA + laser group during a 28-day survival observation period (Fig. 5F), demonstrating outstanding achievement with combined therapy. Moreover, CHASA + laser, CHASA and CHA therapies diminished tumor size without affecting rat weights, and no significant weight differences across groups (Fig. 5G), highlighting the safety of each therapy.

Therapeutic efficacy of CHA and CHASA hydrogels further confirmed by histology and immunofluorescence. H&E staining showed

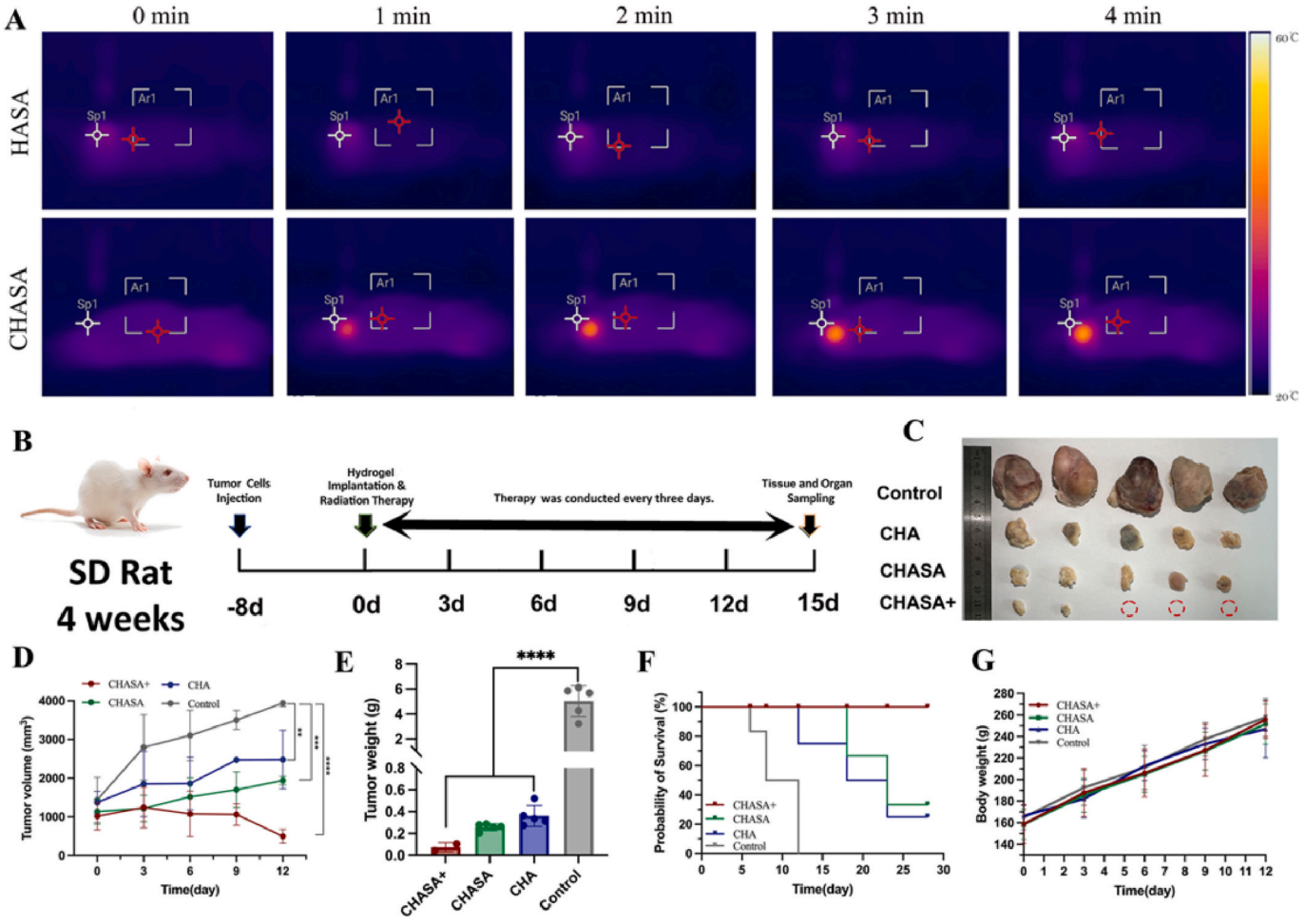

Fig. 5. (A) *In vivo* photothermal effects of CHASA hydrogel after laser irradiation for 4 min. (B)Schedule of osteosarcoma rat models for tumor transplantation and the sequence of hydrogel chemotherapy and radiation therapy. (C) Gross tumor volume size of the extracted tumors in different therapy groups (n = 5). (D) Tumor volume evaluation of the rats (n = 5). (E) Tumor weight of extracted tumors in different therapy groups. (F)Survival probability in different groups (n = 6). (G) Body weight evaluation of the rats in different groups (n = 5). The photothermal laser therapy was conducted under NIR light irradiation (808 nm, 1 W/cm^2). With the data shown as means ± SD. Significant differences among groups were determined by one-way ANOVA and post hoc Dunnett's test; *p < 0.05; **p < 0.01; ***p < 0.001; and ****p < 0.0001.

discontinuities and fragility in hydrogel group tumor tissues (Fig. 6A). Notably, CHASA groups showed sparse, aggregated nuclei, indicating damage to tumor tissue. Furthermore, TUNEL staining was conducted to assess apoptosis levels (Fig. 6B). The control group had lower apoptosis intensities; CHA and CHASA groups showed increased intensities, correlating with tumor tissue disintegration. This suggested an enhanced apoptotic effect induced by CHA and CHASA hydrogels. To further validate the effective activation of the cuproptosis-related pathway, FDX-1 and DLAT levels are measured to validate cuproptosis pathway activation (Fig. 6C). Consistent with late-phase cuproptosis studies, FDX-1 and DLAT levels decreased in CHA, CHASA, and CHASA + laser groups, most in CHASA + laser. This further confirms that SAHA and copper ions triggered FDX-1 and Fe-S cluster aggregation in late-phase osteosarcoma death.

The safety of our intervention was assessed with serum biochemical indicators including ALT, AST, TBIL, UREA, CREA, and UA, revealing no significant differences when compared to those observed in the control group (Fig. 6D).

3.7. Metastasis of the tumor in vitro and in vivo

The anti-tumor metastasis effects of Cu^{2+} and SAHA in HA hydrogel formulations are deeply probed into by integrated methods. Based on the findings from the transwell assay, CHA and CHASA gels effectively impeded tumor cell migration *in vitro*, with CHASA showing the best results (Fig. 7A). In the evaluation of M2 cell polarization rates in Saos-2

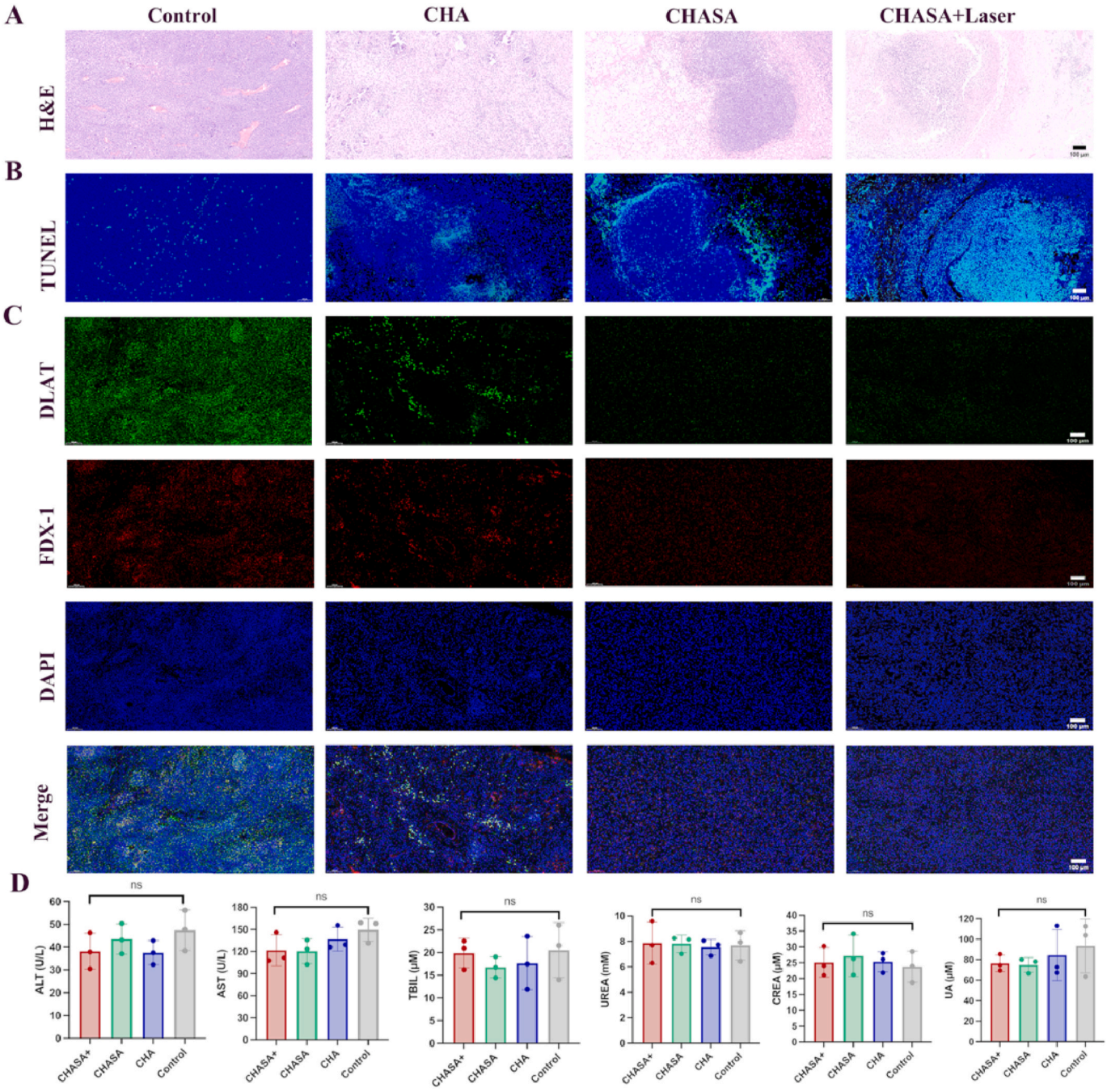

Fig. 6. (A) H&E and (B) TUNEL staining of tumor tissues from the different treatment groups. (C) Immunohistochemical analysis for DLAT, FDX-1 in different groups. Scale bars: 100 μm. (D) Serum biochemical analysis of ALT, AST, TBIL, CREA, UREA and UA in different treatment groups (n = 3). With the data shown as means ± SD. Significant differences among groups were dete rmined by one-way ANOVA and post hoc Dunnett's test.

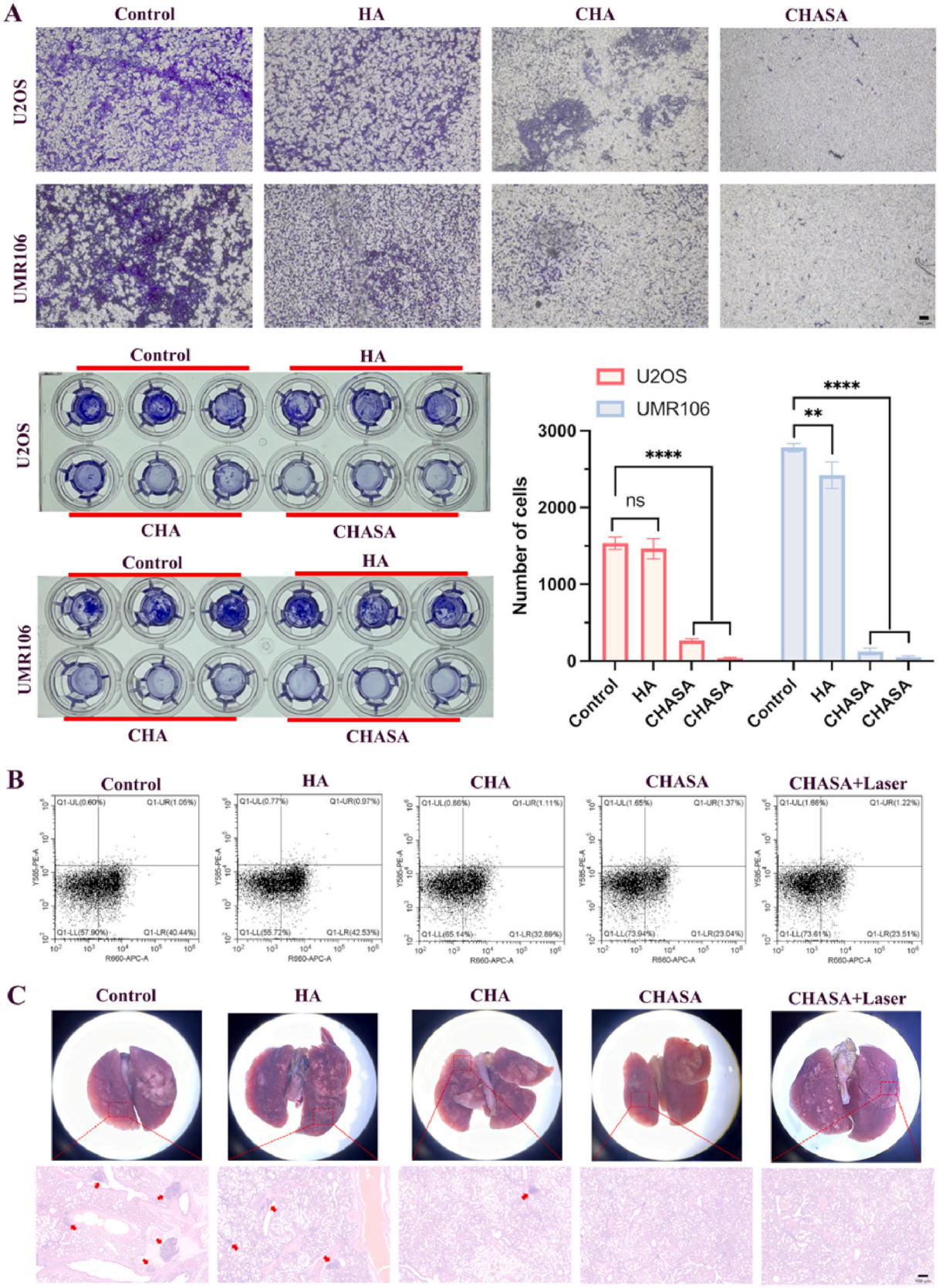

Fig. 7. (A) Transwell results of UMR106 and U2OS treated with saline, HA, CHA, CHASA for 48 h (n=3). (B) Flow cytometry analysis of M2 cell polarization in saos-2 cell lines treated with HA, CHA, CHASA accordingly compared with the control group. (C) Photographs of rat lung tissue and H&E slices of the lung tissue harvested from the rats of osteosarcoma model in different treatment groups. Red arrows, lung metastatic foci. Scale bars: 100 μm. With the data shown as means ± SD. Significant differences among groups were determined by one-way ANOVA and post hoc Dunnett's test; *$p < 0.05$; **$p < 0.01$; ***$p < 0.001$; and ****$p < 0.0001$.

cell lines treated with HA, CHA, and CHASA, both CHA (32.89 %) and CHASA gels (23.04 % without radiation, and 23.51 % with radiation) attenuated the polarization of M0 cells towards M2 (Fig. 7B), thus further restraining the metastatic potential of tumor cells. The anti-metastatic properties of those gels were confirmed in osteosarcoma rat models. CHA group showed reduced metastatic sites, while CHASA and CHASA + laser groups had no metastatic foci, highlighting the potential of SAHA as a cuproptosis enhancer (Fig. 7C).

3.8. The mechanism of CHASA's anti-tumor activity

In our study, the CHASA hydrogel demonstrated remarkable anti-tumor efficacy, with related mechanisms shown in Fig. 8. Upon internalization into tumor cells, the CHASA hydrogel led to a cascade of events. Intracellular GSH and FDX-1 facilitated the reduction of Cu^{2+} to Cu+, subsequently triggering H_2O_2 stimulation for ROS generation. Notably, SAHA synergistically promoted ROS production, augmenting intracellular levels. Moreover, up-regulation of FDX1 not only enhanced free radical generation but also reinforced the early cuproptosis signaling pathway through LIAS up-regulation, thereby promoting cuproptosis progression. Finally, under 808 nm laser irradiation, the CHASA-mediated photothermal effect facilitated the release of Cu^{2+} and SAHA from the hydrogel while inducing tumor cell death via heat shock response. In summary, our designed CHASA hydrogel exhibited exceptional anti-tumor efficacy against osteosarcoma cells through these aforementioned mechanisms.

4. Conclusion

This work originates from the clinical demand for novel combined osteosarcoma treatments. Our initial approach has centered on localized injection-induced thermotherapy using copper ions. However, we find that intracellular copper levels, regulated by copper-binding ionophores, limited the therapeutic efficacy. By introducing L-cysteine to sequester copper ions and hyaluronate to elevate intracellular copper levels, we develop cuproptosis-induced osteosarcoma photothermal treatment in rats within a novel hydrogel, $SAHA_m$@{[Cu(HA-Cys)$_2$]Cl_2}$_n$ (CHASA), eliminating surgical intervention for 2 weeks. Copper-based hydrogels stand out for tumor therapies due to tunable formulations, copper-induced cell death, ROS generation, and photothermal compatibility. While SAHA shows powerful versatility in various combining therapies, our study reveals SAHA's upregulation of FDX-1 in cuproptosis, enabling the in-situ injection gel regressing osteosarcoma and inhibiting metastasis in rats. Therefore, with integrating copper and SAHA into a hyaluronic acid matrix, our in-situ injection hydrogel shows promising prospect for clinical translation of cuproptosis-mediated photothermal therapy, offering potential strategy against the devasting osteosarcoma.

Funding

This work was supported by the National Natural Science Foundation of China (No. 82473891, 82072421, 82304455), Naval Key Discipline Group Construction Project (2024-HJZDXK-YC-06), the Shanghai Sailing Program (21YF1457700, 23YF1457600), the Naval Medical University Cultivation Foundation for General Project (2022MS005, 2023MS009) and Basic Medicine School of Naval Medical University (JCKFKT-ZD-001).

CRediT authorship contribution statement

Sizhen Wang: Writing – original draft, Visualization, Validation, Methodology, Investigation, Formal analysis, Data curation, Conceptualization. **Hanzhe Zhang:** Writing – original draft, Visualization,

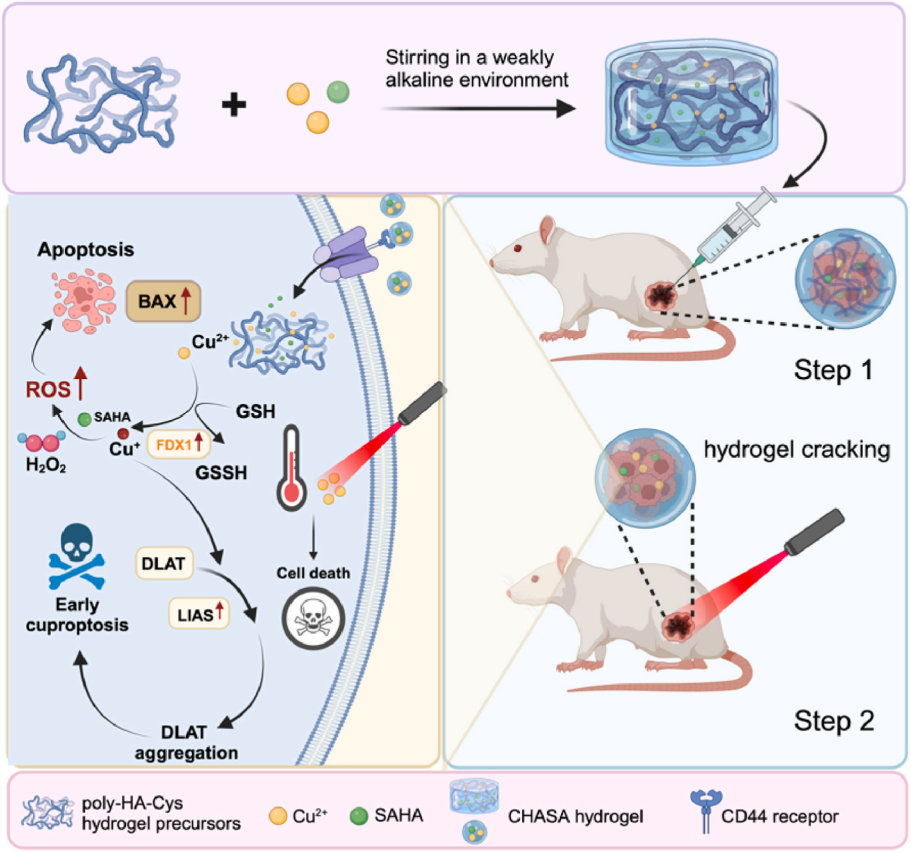

Fig. 8. The antitumor mechanism of CHASA hydrogel (created with Biorender.com).

Validation, Methodology, Investigation, Formal analysis, Data curation, Conceptualization. **Tianheng Chen:** Software, Methodology, Investigation, Formal analysis, Data curation, Conceptualization. **Weiwei Jiang:** Methodology, Investigation, Formal analysis. **Feng Wang:** Methodology, Investigation, Formal analysis. **Yuhao Yu:** Methodology, Investigation, Funding acquisition. **Beibei Guo:** Methodology, Investigation, Funding acquisition. **Jia Xu:** Methodology, Investigation. **Feng Yang:** Validation, Supervision, Resources, Funding acquisition. **Qinglin Kang:** Validation, Supervision, Project administration, Methodology, Funding acquisition, Formal analysis, Conceptualization. **Zhiqiang Ma:** Writing – review & editing, Validation, Supervision, Project administration, Methodology, Funding acquisition, Formal analysis, Conceptualization.

Declaration of competing interest

The authors declare that they have no known competing financial interests or personal relationships that could have appeared to influence the work reported in this paper.

Appendix A. Supplementary data

Supplementary data to this article can be found online at https://doi.org/10.1016/j.mtbio.2024.101368.

Data availability

Data will be made available on request.

References

[1] G. Ottaviani, N. Jaffe, The epidemiology of osteosarcoma, Cancer Treat Res. 152 (2009) 3–13.
[2] S. Cole, D.M. Gianferante, B. Zhu, et al., Osteosarcoma: a surveillance, epidemiology, and end results program-based analysis from 1975 to 2017, Cancer 128 (11) (2022) 2107–2118.
[3] M.P. Link, A.M. Goorin, A.W. Miser, et al., The effect of adjuvant chemotherapy on relapse-free survival in patients with osteosarcoma of the extremity, N. Engl. J. Med. 314 (25) (1986) 1600–1606.
[4] N. Esiashvili, M. Goodman, R.J. Marcus, Changes in incidence and survival of Ewing sarcoma patients over the past 3 decades: surveillance Epidemiology and End Results data, J. Pediatr. Hematol. Oncol. 30 (6) (2008) 425–430.
[5] L. Mirabello, R.J. Troisi, S.A. Savage, Osteosarcoma incidence and survival rates from 1973 to 2004: data from the surveillance, epidemiology, and end results program, Cancer 115 (7) (2009) 1531–1543.
[6] L. Mirabello, R.J. Troisi, S.A. Savage, International osteosarcoma incidence patterns in children and adolescents, middle ages and elderly persons, Int. J. Cancer 125 (1) (2009) 229–234.
[7] K. Yahiro, Y. Matsumoto, Immunotherapy for osteosarcoma, Hum. Vaccines Immunother. 17 (5) (2021) 1294–1295.
[8] V.A. Li, C. Scialabba, V. Vetri, et al., Near-infrared light responsive folate targeted gold nanorods for combined photothermal-chemotherapy of osteosarcoma, ACS Appl. Mater. Interfaces 9 (16) (2017) 14453–14469.
[9] J.A. Perry, A. Kiezun, P. Tonzi, et al., Complementary genomic approaches highlight the PI3K/mTOR pathway as a common vulnerability in osteosarcoma, Proc. Natl. Acad. Sci. U. S. A. 111 (51) (2014) E5564–E5573.
[10] A. Gupte, E.K. Baker, S.S. Wan, et al., Systematic screening identifies dual PI3K and mTOR inhibition as a conserved therapeutic vulnerability in osteosarcoma, Clin. Cancer Res. 21 (14) (2015) 3216–3229.
[11] K. Chen, S. Fallen, H.O. Abaan, et al., Wnt10b induces chemotaxis of osteosarcoma and correlates with reduced survival, Pediatr. Blood Cancer 51 (3) (2008) 349–355.
[12] S.D. Goldstein, M. Trucco, G.W. Bautista, et al., A monoclonal antibody against the Wnt signaling inhibitor dickkopf-1 inhibits osteosarcoma metastasis in a preclinical model, Oncotarget 7 (16) (2016) 21114–21123.
[13] S.D. Molyneux, M.A. Di Grappa, A.G. Beristain, et al., Prkar1a is an osteosarcoma tumor suppressor that defines a molecular subclass in mice, J. Clin. Invest. 120 (9) (2010) 3310–3325.
[14] A.J. Saraf, J.M. Fenger, R.D. Roberts, Osteosarcoma: accelerating progress makes for a hopeful future, Front. Oncol. 8 (2018) 4.
[15] B.S. Moriarity, G.M. Otto, E.P. Rahrmann, et al., A Sleeping Beauty forward genetic screen identifies new genes and pathways driving osteosarcoma development and metastasis, Nat. Genet. 47 (6) (2015) 615–624.
[16] P. Tsvetkov, S. Coy, B. Petrova, et al., Copper induces cell death by targeting lipoylated TCA cycle proteins, Science 375 (6586) (2022) 1254–1261.
[17] M.B. Dreishpoon, N.R. Bick, B. Petrova, et al., FDX1 regulates cellular protein lipoylation through direct binding to LIAS, J. Biol. Chem. 299 (9) (2023) 105046.
[18] Q. Xue, R. Kang, D.J. Klionsky, et al., Copper metabolism in cell death and autophagy, Autophagy 19 (8) (2023) 2175–2195.
[19] Y. Zhang, Q. Zhou, L. Lu, et al., Copper induces cognitive impairment in mice via modulation of cuproptosis and CREB signaling, Nutrients 15 (4) (2023).
[20] A. Solmonson, R.J. DeBerardinis, Lipoic acid metabolism and mitochondrial redox regulation, J. Biol. Chem. 293 (20) (2018) 7522–7530.
[21] E.A. Rowland, C.K. Snowden, I.M. Cristea, Protein lipoylation: an evolutionarily conserved metabolic regulator of health and disease, Curr. Opin. Chem. Biol. 42 (2018) 76–85.
[22] B.E. Kim, T. Nevitt, D.J. Thiele, Mechanisms for copper acquisition, distribution and regulation, Nat. Chem. Biol. 4 (3) (2008) 176–185.
[23] E.J. Ge, A.I. Bush, A. Casini, et al., Connecting copper and cancer: from transition metal signalling to metalloplasia, Nat. Rev. Cancer 22 (2) (2022) 102–113.
[24] S. Lutsenko, Human copper homeostasis: a network of interconnected pathways, Curr. Opin. Chem. Biol. 14 (2) (2010) 211–217.
[25] S. Solier, S. Muller, T. Caneque, et al., A druggable copper-signalling pathway that drives inflammation, Nature 617 (7960) (2023) 386–394.
[26] S. Muller, F. Sindikubwabo, T. Caneque, et al., CD44 regulates epigenetic plasticity by mediating iron endocytosis, Nat. Chem. 12 (10) (2020) 929–938.
[27] R.S. Benjamin, Adjuvant and neoadjuvant chemotherapy for osteosarcoma: a historical perspective, Adv. Exp. Med. Biol. 1257 (2020) 1–10.
[28] S. Tsukamoto, A. Righi, A. Kido, et al., Effect of adjuvant chemotherapy on periosteal osteosarcoma: a systematic review, Jpn. J. Clin. Oncol. 52 (8) (2022) 896–904.
[29] D. Carrle, S.S. Bielack, Current strategies of chemotherapy in osteosarcoma, Int. Orthop. 30 (6) (2006) 445–451.
[30] S. Ferrari, S. Smeland, M. Mercuri, et al., Neoadjuvant chemotherapy with high-dose Ifosfamide, high-dose methotrexate, cisplatin, and doxorubicin for patients with localized osteosarcoma of the extremity: a joint study by the Italian and Scandinavian Sarcoma Groups, J. Clin. Oncol. 23 (34) (2005) 8845–8852.
[31] A. Longhi, C. Errani, M. De Paolis, et al., Primary bone osteosarcoma in the pediatric age: state of the art, Cancer Treat Rev. 32 (6) (2006) 423–436.
[32] A. Pettke, M. Hotfilder, D. Clemens, et al., Suberanilohydroxamic acid (vorinostat) synergistically enhances the cytotoxicity of doxorubicin and cisplatin in osteosarcoma cell lines, Anti Cancer Drugs 27 (10) (2016) 1001–1010.
[33] X. Zhou, Z. Liu, H. Wang, et al., SAHA (vorinostat) facilitates functional polymer-based gene transfection via upregulation of ROS and synergizes with TRAIL gene delivery for cancer therapy, J. Drug Target. 27 (3) (2019) 306–314.
[34] C. Blattmann, S. Oertel, V. Ehemann, et al., Enhancement of radiation response in osteosarcoma and rhabdomyosarcoma cell lines by histone deacetylase inhibition, Int. J. Radiat. Oncol. Biol. Phys. 78 (1) (2010) 237–245.
[35] S.D. Bhagat, U. Singh, R.K. Mishra, et al., An endogenous reactive oxygen species (ROS)-Activated histone deacetylase inhibitor prodrug for cancer chemotherapy, ChemMedChem 13 (19) (2018) 2073–2079.
[36] X. Mu, D. Brynien, K.R. Weiss, The HDAC inhibitor Vorinostat diminishes the in vitro metastatic behavior of Osteosarcoma cells, BioMed Res. Int. 2015 (2015) 290368.
[37] L. Ramos, S. Truong, B. Zhai, et al., A bifunctional PARP-HDAC inhibitor with activity in ewing sarcoma, Clin. Cancer Res. 29 (17) (2023) 3541–3553.
[38] S. Hesse, T.N. Wassermann, M.A. Suhm, Brightening and locking a weak and floppy N-H chromophore: the case of pyrrolidine, J. Phys. Chem. A 114 (39) (2010) 10492–10499.
[39] K. Shimada, E. Reznik, M.E. Stokes, et al., Copper-binding small molecule induces oxidative stress and cell-cycle arrest in glioblastoma-patient-derived cells, Cell Chem. Biol. 25 (5) (2018) 585–594.
[40] M. Nagai, N.H. Vo, O.L. Shin, et al., The oncology drug elesclomol selectively transports copper to the mitochondria to induce oxidative stress in cancer cells, Free Radic. Biol. Med. 52 (10) (2012) 2142–2150.
[41] J. Casteel, J.A. Miernyk, J.J. Thelen, Mapping the lipoylation site of Arabidopsis thaliana plastidial dihydrolipoamide S-acetyltransferase using mass spectrometry and site-directed mutagenesis, Plant Physiol. Biochem. 49 (11) (2011) 1355–1361.
[42] P. Tsvetkov, S. Coy, B. Petrova, et al., Copper induces cell death by targeting lipoylated TCA cycle proteins, Science 375 (6586) (2022) 1254–1261.